Acta Crystallographica Section D
Biological Crystallography
ISSN 0907-4449

Nucleotide-binding flexibility in ultrahigh-resolution structures of the SRP GTPase Ffh

Ursula D. Ramirez,‡ Pamela J. Focia and Douglas M. Freymann*

Department of Molecular Pharmacology and Biological Chemistry, Northwestern University, Chicago, IL 60611, USA

‡ Current address: Biomolecular Structure and Function, Basic Science Division, Fox Chase Cancer Center, Philadelphia, Pennsylvania, USA.

Correspondence e-mail: freymann@northwestern.edu

Received 6 June 2008
Accepted 30 July 2008

PDB References: GDP-bound Ffh NG domain, 2c03, r2c03sf; GMPPCP-bound Ffh NG domain, 2c04, r2c04sf.

Two structures of the nucleotide-bound NG domain of Ffh, the GTPase subunit of the bacterial signal recognition particle (SRP), have been determined at ultrahigh resolution in similar crystal forms. One is GDP-bound and one is GMPPCP-bound. The asymmetric unit of each structure contains two protein monomers, each of which exhibits differences in nucleotide-binding conformation and occupancy. The GDP-bound Ffh NG exhibits two binding conformations in one monomer but not the other and the GMPPCP-bound protein exhibits full occupancy of the nucleotide in one monomer but only partial occupancy in the other. Thus, under the same solution conditions, each crystal reveals multiple binding states that suggest that even when nucleotide is bound its position in the Ffh NG active site is dynamic. Some differences in the positioning of the bound nucleotide may arise from differences in the crystal-packing environment and specific factors that have been identified include the relative positions of the N and G domains, small conformational changes in the P-loop, the positions of waters buried within the active site and shifts in the closing loop that packs against the guanine base. However, 'loose' binding may have biological significance in promoting facile nucleotide exchange and providing a mechanism for priming the SRP GTPase prior to its activation in its complex with the SRP receptor.

1. Introduction

The signal recognition particle (SRP) GTPases Ffh and FtsY function in co-translational targeting of nascent polypeptides to the membrane translocon (Keenan *et al.*, 2001; Luirink & Dobberstein, 1994; Luirink & Sinning, 2004; Pool, 2005). Both proteins contain a structurally homologous GTPase, termed the NG domain, which is similar to other members of the GTPase superfamily (G) but contains two insertions relative to the Ras-like GTPase fold: a four α-helical bundle at the N-terminus (N) and an insertion-box subdomain (IBD) comprising two β-strands and two α-helices that includes the second of four conserved GTPase motifs (Freymann *et al.*, 1997, 1999). These conserved motifs (Bourne *et al.*, 1991; Wittinghofer & Gierschik, 2000) include the P-loop (motif I), which interacts with the phosphates of the GTP, motif II (also called switch 1) and motif III (also called switch 2), which interact with the γ-phosphate of the nucleotide and undergo conformational changes upon changes in nucleotide-binding state, and motif IV, which hydrogen bonds the guanine base. Additional sequence motifs are unique to the SRP GTPases. The DARGG and ALLEADV motifs are at the N/G interface. The DARGG motif (Asp250–Leu257) follows motif IV in the

protein sequence in the α4 helix of the G domain and the ALLEADV motif (Ala37–Val43) is located across the interface from the DARGG motif in a loop of the N domain (Freymann *et al.*, 1997, 1999). Together with the DAGQ motif (Asp219–Gln224; Focia, Shepotinovskaya *et al.*, 2004), these contribute to a series of symmetric interactions which generate much of the interface of Ffh with its receptor FtsY when they form their pseudo-symmetric targeting complex (Egea *et al.*, 2004; Focia, Shepotinovskaya *et al.*, 2004). Finally, the 'closing loop' (Gly271–Gly278), adjacent to the active site, is poorly structured and can undergo large conformational change to pack against the guanine base when nucleotide is bound.

The structures of the NG domain of Ffh from *Thermus aquaticus* in its GDP-bound (PDB code 2ng1), Mg^{2+}GDP-bound (PDB code 1ng1) and GMPPNP-bound (PDB code 1jpn) states have been determined previously at ~2.0 Å resolution (Freymann *et al.*, 1999; Padmanabhan & Freymann, 2001). Nucleotide binding to the SRP GTPases has some unique elements. While the interactions with the guanine base and the binding mode for Mg^{2+}GDP are similar to those observed in other GTPase structures, monomeric Ffh NG can bind GDP in an Mg^{2+}-free configuration that is distinct, involving extrusion of the β-phosphate away from the P-loop (Freymann *et al.*, 1999), and it binds GMPPNP in a related configuration unique to SRP GTPases in which the β-phosphate is displaced from the P-loop and the γ-phosphate turned back towards it (Padmanabhan & Freymann, 2001). Only on formation of the heterodimeric complex, which is mediated in part by interactions across the binding sites of the NG domains of both Ffh and FtsY, has the nucleotide been observed to adopt the canonical extended binding configuration observed in other GTP-bound GTPase structures (Egea *et al.*, 2004; Focia, Shepotinovskaya *et al.*, 2004).

Two new structures, one of Ffh NG bound to Mg^{2+}-free GDP and one of Ffh NG bound to the nonhydrolysable GTP analog GMPPCP, were obtained under different solution and precipitant conditions but in the same crystal form that diffracted to better than 1.2 Å resolution. There are two monomers in the asymmetric unit and there are clear differences in the nature of nucleotide binding between the structures. These atomic resolution structures provide additional insight into nucleotide binding in the SRP GTPases. Specific differences in binding configuration and occupancy can be related in part to differences in the crystal-packing environments of the two molecules in the asymmetric unit. These provide snapshots of nucleotide-binding dynamics that illustrate how subtle differences in the protein and water structure at the binding site contribute to relatively large differences in binding configuration. The structures directly illustrate the 'loose' nature of nucleotide binding to the SRP GTPase Ffh, consistent with the functionally important observation that the binding mode is not fixed prior to interaction with the receptor (Padmanabhan & Freymann, 2001; Rapiejko & Gilmore, 1997; Song *et al.*, 2000). In the receptor complex GTP is completely buried at the symmetric interface and the two nucleotides of the complex interact directly (Egea *et al.*, 2004; Focia, Shepotinovskaya *et al.*, 2004). Exploiting the high-resolution structures of the nucleotide-bound species allows us to begin to discern the specific protein structural interactions that dictate these distinct binding configurations.

2. Materials and methods

2.1. Crystallization

Ffh NG was expressed and purified as described previously (Freymann *et al.*, 1997; Shepotinovskaya *et al.*, 2003). Crystals of the GDP-bound Ffh NG domain were grown by the addition of 2 µl mother liquor consisting of 30% dioxane to 2 µl 28.5 mg ml^{-1} Ffh NG (residues 1–297) in 2 m*M* GDP. Crystallization by hanging-drop vapor diffusion was carried out at room temperature and 20% ethylene glycol was added to the mother liquor before the crystal was harvested and mounted using a nylon loop and flash-cooled in liquid nitrogen (Teng, 1990). Crystals of the GMPPCP-bound Ffh NG domain were grown by the addition of 2 µl mother liquor, which consisted of 30% MPD, 0.1 *M* sodium acetate pH 4.7, 20 m*M* $CaCl_2$, 0.15 *M* potassium acetate, to 2 µl 22 mg ml^{-1} Ffh NG 1–297 in 2 m*M* $MgCl_2$ and 2 m*M* GMPPCP. Crystallization by sitting-drop vapor diffusion was carried out at 277 K. It was necessary to use cross-dilution streak-seeding to limit nucleation. After 1 d incubation at 277 K, the crystallization drops were streak-seeded from a stock grown under similar conditions to obtain large (to 1 mm) single crystals (Stura & Wilson, 1990, 1991). For data collection, a crystal (1 × 0.4 × 0.5 mm) was mounted directly from its mother liquor using a nylon loop and flash-cooled in liquid nitrogen (Teng, 1990).

2.2. Data collection and processing

Data from crystals of GDP-bound Ffh NG (structure DP) were measured using a MAR CCD detector on the DND-CAT beamline 5-ID-B at a wavelength of 0.7429 Å. Data from crystals of GMPPCP-bound Ffh NG (structure PCP) were measured on the BioCARS beamline 14-BM-C using an ADSC Quantum-4 detector at a wavelength of 0.90 Å. Data for structure DP were measured in two overlapping resolution ranges and data for structure PCP were measured in three overlapping resolution ranges. For structure DP, the high-resolution data were measured in dose mode at a crystal-to-detector distance of 85 mm and with an exposure time of approximately 30 s per 0.5° oscillation frame and the low-resolution data were measured with an exposure time of approximately 5 s per 2° oscillation. For structure PCP, the high-resolution data were measured in dose mode at a crystal-to-detector distance of 85 mm and with an exposure time of approximately 14 s per 0.5° oscillation, the medium-resolution data were measured with an exposure time of ~2 s per 1.0° oscillation and the low-resolution data were measured with an exposure time of ~1.4 s per 2° oscillation. Data for both structures were integrated using *DENZO* and scaled using *SCALEPACK* (Otwinowski, 1993) with a -3σ cutoff. Statistics of the data are shown in Table 1.

Table 1
Data-collection and refinement statistics.

Values in parentheses are for the last resolution shell.

	GMPPCP–Ffh NG	GDP–Ffh NG
Data collection		
Space group	*C*2	*C*2
Unit-cell parameters		
a (Å)	109.01	108.59
b (Å)	54.44	55.11
c (Å)	98.83	96.11
β (°)	97.16	101.73
Resolution range (Å)	19.6–1.14 (1.17–1.14)	50.0–1.24 (1.27–1.24)
Unique reflections	192311	154602
$R_{\rm merge}$† (%)	5.6 (36.1)	6.3 (47.4)
Completeness (%)	94.3 (90.9)	94.9 (96.1)
Redundancy	4.5 (3.0)	3.6 (3.0)
Average $I/\sigma(I)$	29.7 (3.4)	12.5 (2.0)
Refinement		
No. of test-set reflections	12239	8982
$R_{\rm cryst}$‡ (%)	14.4	13.3
$R_{\rm free}$ (%)	17.7	18.6
No. of protein atoms	4568	4548
No. in alternative conformations	3797	1293
No. of water molecules	561	594
No. in alternative conformations	9	25
No. of alternate-conformation residues	*A*, 194; *B*, 297§	*A*, 74; *B*, 82
Average temperature factor (Å^2)		
Protein	19.9	22.8
Water	30.4	33.8
Alternate conformations	18.8	25.9
Nucleotide	21.9	19.5
R.m.s.d. bond lengths (Å)	0.010	0.013
R.m.s.d. bond angles (°)	1.737	1.603

† $R_{\rm merge} = 100 \times \sum_{hkl} \sum_i |I_i(hkl) - \langle I(hkl)\rangle| / \sum_{hkl} \sum_i I_i(hkl)$, where $\langle I(hkl)\rangle$ is the average intensity over symmetry equivalents. ‡ $R_{\rm cryst} = 100 \times \sum |F_{\rm o} - F_{\rm c}| / \sum F_{\rm o}$. § Refined as two complete polypeptide chains.

2.3. Crystallographic refinement

For the GDP-bound structure (DP), PDB entry 1ffh was used as the initial phasing model and the structure was determined by molecular replacement using *AMoRe*. The initial solution was refined using *X-PLOR* rigid-body and positional protocols. For the GMPPCP-bound Ffh NG structure (PCP), the structure of the GMPPNP complex of Ffh NG (PDB code 1jpn; Padmanabhan & Freymann, 2001), which crystallizes under similar conditions, was used as the initial phasing model following removal of all solvent and ligand atoms. Rigid-body refinement using *REFMAC* (Murshudov *et al.*, 1997, 1999) and data in the resolution range 15–3 Å were used to position the model, followed by 30 cycles of positional refinement over the resolution range 19.96–1.24 Å for structure DP and 19.65–1.15 Å for structure PCP. An initial set of solvent atoms was added to each structure using *ARP*/*wARP* (Lamzin *et al.*, 2001; Perrakis *et al.*, 1999). The models were inspected and rebuilt manually using *O* (Jones *et al.*, 1991). In structure PCP, negative density upon addition of a GMPPCP molecule at full occupancy in monomer *B* indicated that the nucleotide is not at full occupancy and its occupancy was estimated based upon examination of residual density maps. Subsequently, refinement with *REFMAC* (Murshudov *et al.*, 1997, 1999) incorporated anisotropic displacement parameters and a bulk-solvent model. Electron-density maps were calculated using the *CCP*4 suite (Collaborative Computational Project, Number 4, 1994).

2.4. Alternate conformations and radiation damage

Alternate conformations were managed using locally written scripts and the program *ACONIO* (Kleywegt *et al.*, 2001). The entire first conformation of the *B* monomer of a previously published apo Ffh NG structure (PDB code 2j45; Ramirez & Freymann, 2006), which is of similar resolution and in the same crystal form as structure PCP, was substituted for the 77 residues in alternate conformations as the second (apo) conformation of the *B* monomer of structure PCP. However, upon further substitution of the complete apo model as a partially occupied second conformation the $R_{\rm free}$ dropped by about 1%, suggesting that the complete model fitted the data better than a partial second conformation built from the nucleotide-bound conformation. Thus, the structure was modeled as two complete chains at 60% (nucleotide-bound) and 40% (apo) occupancy (DePristo *et al.*, 2004).

Radiation damage was clearly evident at some glutamate and methionine side chains (Burmeister, 2000; Teng & Moffat, 2002; Weik *et al.*, 2000). These side chains were modeled by setting the atoms of the terminal carboxylate groups of glutamate and the terminal thiomethyl groups of methionine to partial occupancy. In structure DP nine glutamate residues and two methionine residues exhibited radiation damage and in structure PCP there are 15 such glutamates and one methionine. Interestingly, only four residues, all glutamates, are damaged in common between the *A* and *B* monomers; these are in structure PCP.

Coordinates were evaluated with *MOLPROBITY* (Lovell *et al.*, 2003) and 100% of the residues are in allowed regions, with 99.49% of the residues of structure DP in favored regions and 98.64% of residues of structure PCP in favored regions. Chain assignments for the two monomers in the asymmetric units of both structures are consistent with all structures of this crystal form, including previously published structures (PDB codes 2j45, 2j46 and 1jpn; Padmanabhan & Freymann, 2001; Ramirez & Freymann, 2006), according to crystal-packing interactions as determined using the *CCP*4 program *ACT* (Collaborative Computational Project, Number 4, 1994). In structure DP, in addition to the GDP and water, several nonwater solvent molecules from crystallization and cryoprotectant solutions were identified; two are ethylene glycol molecules and 14 are dioxane molecules. In structure PCP, two calcium ions were also identified. Despite the availability of high concentrations of Mg^{2+} and Ca^{2+} in the PCP crystallization conditions, the Mg^{2+}-binding position in the GTPase active site is not occupied. Refinement statistics are presented in Table 1.

2.5. Structural analysis

Structures were superimposed and r.m.s.d.s and displacement distances between C^{α} atoms were calculated with the *LSQMAN* 'Brute-force' option followed by the 'Improve'

option over 173 C^{α} atoms (99–171) of the G domains. The 'Improve' option was then applied over the 16 C^{α} atoms of the P-loop (residues 105–117) to calculate r.m.s.d.s and displacement distances for the C^{α} atoms of the P-loop (Table 2). To generate crystal-contact information, symmetry-related atoms within 15 Å of atoms within the working asymmetric unit were generated using *XPAND* (Kleywegt & Jones, 1997) and explicit hydrogen positions were added to the symmetry-related atoms using *REDUCE* (Word, Lovell, LaBean *et al.*, 1999). Contact dots were generated using the program *PROBE* (Lovell *et al.*, 1999), which simulates rolling a spherical probe of 0.25 Å radius across the van der Waals surface of atoms and leaves an indication (contact dot) where two surfaces are closer than 0.5 Å. *PROBE* was also used to generate contact dots for intramolecular packing interactions excluding solvent and nucleotide atoms. Contact dots of surface residues were eliminated from the packing analysis. Figures were generated using *MOLSCRIPT* (Kraulis, 1991) and *RASTER3D* (Merritt & Bacon, 1997).

3. Results and discussion

3.1. High-resolution structures of the nucleotide-bound SRP GTPase

The structures of GDP-bound Ffh NG, here termed structure DP, and GMPPCP-bound Ffh NG, here termed structure PCP, were obtained from the same crystal form which crystallized under different precipitant and buffer conditions (see §2). Structure DP, at 1.24 Å resolution, was refined to an $R_{\rm cryst}$ of 13.3% and an $R_{\rm free}$ of 18.6% and structure PCP, at 1.14 Å resolution, refined to an $R_{\rm cryst}$ of 14.4% and an $R_{\rm free}$ of 17.7% (Table 1). The improvement in $R_{\rm cryst}$ and $R_{\rm free}$ for the final models of structure DP following incorporation of anisotropic temperature factors was 4.2% and 2.9% for $R_{\rm cryst}$ and $R_{\rm free}$, respectively, and for structure PCP was 3.3% and 2.3%, respectively, values that are typical for structures of this resolution (Schneider, 1996; Walsh *et al.*, 1998). The electron-density maps are of very high quality and the residual difference density indicates that no major features were overlooked. Thus, omission of a fully occupied water molecule from the final model leaves a positive difference peak of approximately 11σ and an omitted P atom leaves a positive residual difference peak of approximately 18σ. In comparison, the highest positive and negative difference peaks remaining in structure DP are 5.3σ and −4.7σ, respectively. The positive difference peak is located near a twofold axis and cannot be modeled as water or any other solvent molecule and the highest negative residual difference peak is located in the solvent space near Lys62 (however, no atoms were modeled at this position). In structure PCP, the highest positive residual difference peak is 5.7σ and is located along the main chain between Arg170 and Arg171, but is not interpretable as alternate main-chain conformations. The highest negative peak in the residual difference map is −4.6σ near the NE atom of the Arg35 side chain. In both structures, all residues are in the allowed region of the Ramachandran plot (Lovell *et al.*, 2003).

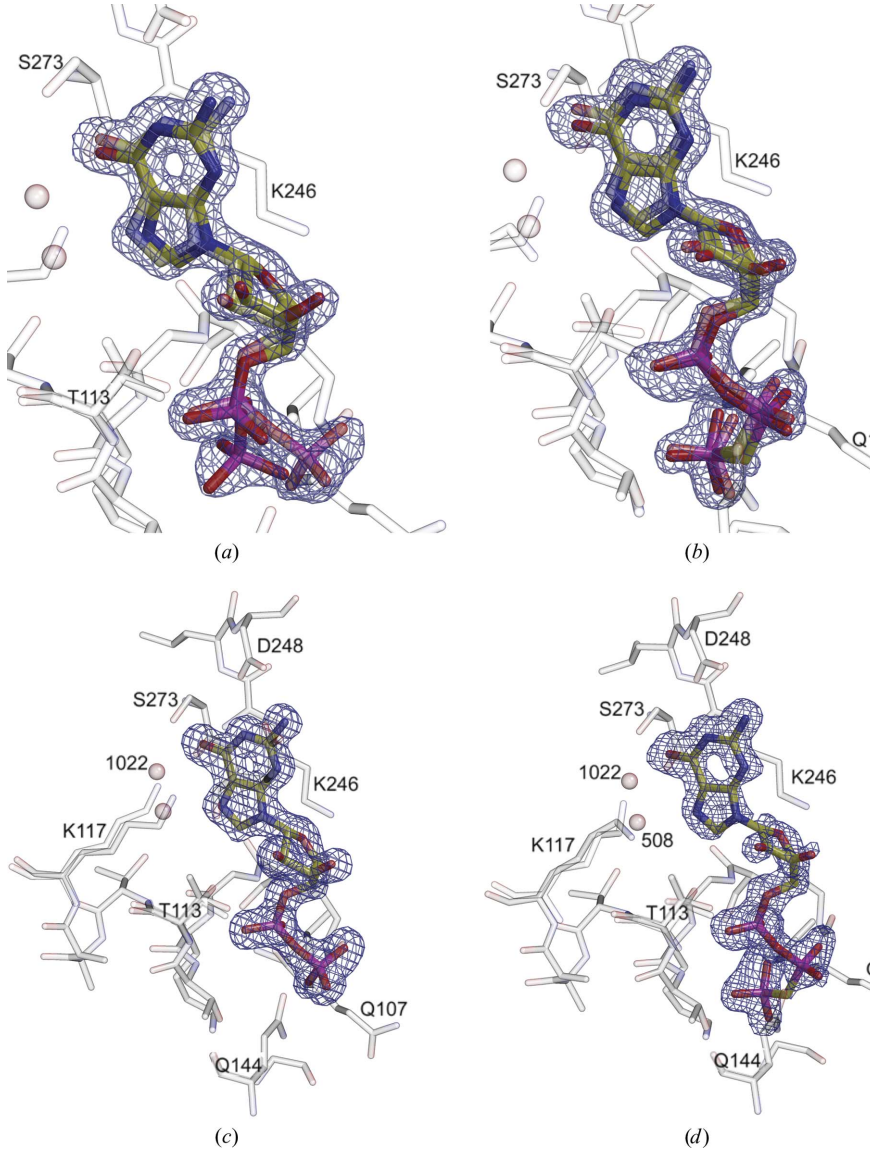

Figure 1
Nucleotide-binding configurations. $F_{\rm o} - F_{\rm c}$ density maps calculated with nucleotides omitted from the model are shown contoured at 3σ and superimposed with the corresponding nucleotide and surrounding protein residues. (*a*) Monomer *A* of structure DP. The canonical extended GDP (configuration 1) is shown in full color and the alternative 'flipped-out' GDP (configuration 2) is shown in faded colors. (*b*) Monomer *A* of structure PCP. (*c*) Monomer *B* of structure DP. Surrounding residues, including alternate conformations of Lys117 and Thr113, and the nucleotide model are superimposed. (*d*) Monomer *B* of structure PCP. Relatively poor definition of the density here arises from partial occupancy of the site.

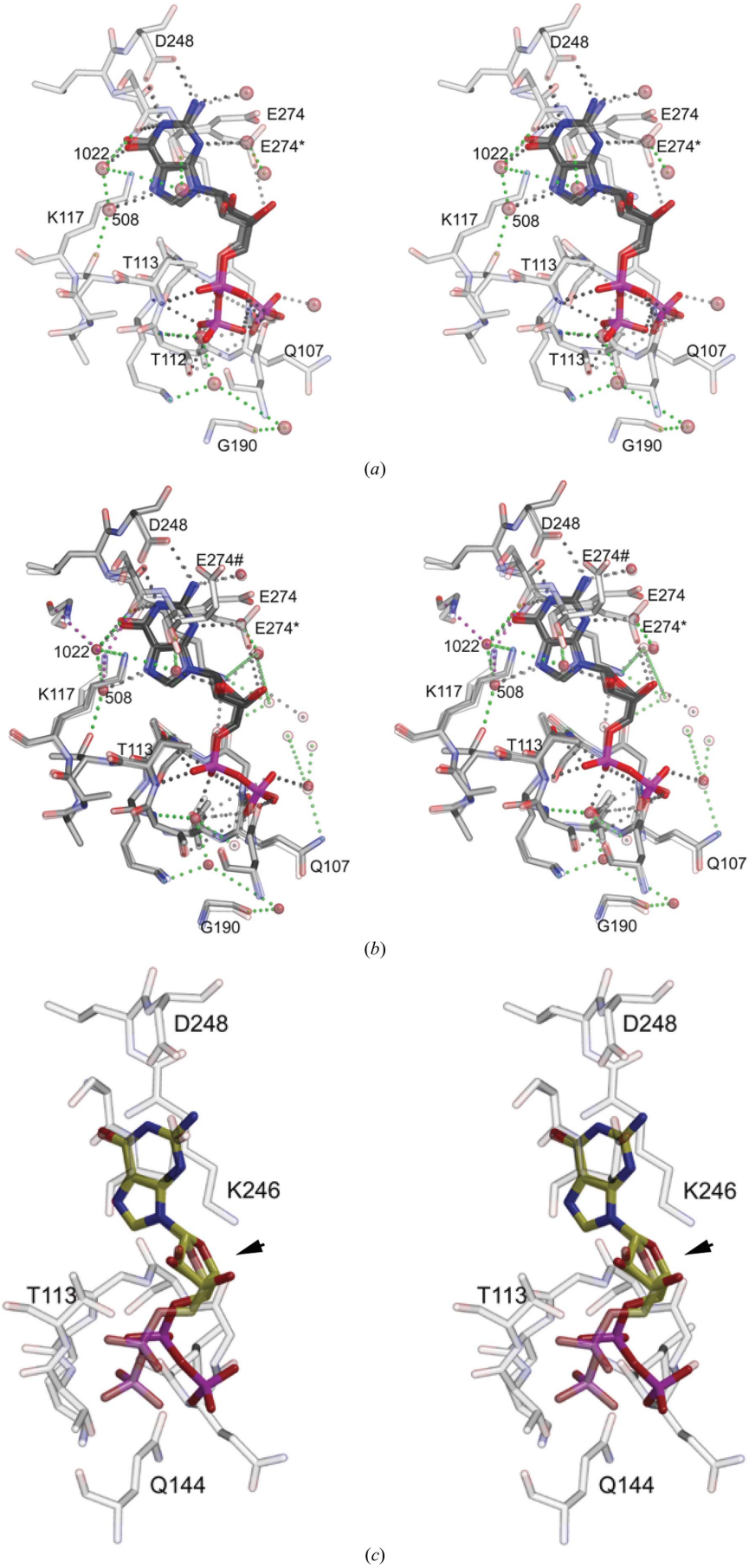

An extensive crystal-packing interface that generates a twofold-related (but not physiological) dimer across one or the other of two distinct crystallographic twofold axes within the *C*2 unit cell is common to both monomers in the asymmetric unit, but other packing interactions are unique to each. In both structures the nucleotide-binding modes differ between the two monomers and are heterogeneous within at least one of the two unique sites of each crystal form. Because of the quality of the diffraction data and the high resolution of the structures, there is clear evidence for variation in the nucleotide-binding configuration, which we have modeled as alternate binding configurations, including torsional and translational shifts and partial occupancy at one binding site. A key factor that contributes to enabling this analysis is that the apo configuration of the protein is similar to that of the GDP and GMPPCP-bound monomeric states (Focia, Alam *et al.*, 2004; Padmanabhan & Freymann, 2001; Reyes *et al.*, 2007).

Figure 2
Comparison of GDP-binding interactions. Stereo diagrams of hydrogen-bonding networks in the active sites of the *A* and *B* monomers are shown. (*a*) Conformation 1 of GDP in monomer *A* is shown in full colors and configuration 2 is shown in faded colors. Hydrogen bonds between each of the nucleotides and the surrounding residues and solvent molecules are shown in full colors. Hydrogen bonds between residues and water molecules that directly interact with the nucleotide are shown in black for conformation 1 and in gray for conformation 2. (*b*) Hydrogen bonds between conformation 2 of GDP in monomer *A* of structure DP and the surrounding residues and solvent molecules are shown in black and hydrogen bonds between GDP in monomer *B* of structure DP and the surrounding residues and solvent molecules are shown in grey. Residues and nucleotide of monomer *A* are shown in full colors and those of monomer *B* are shown in faded colors. Hydrogen bonds between surrounding protein and solvent structure are shown in light green. An alternate conformation of Lys117 is shown and its interactions in this conformation are shown as magenta dotted lines. (*c*) The extended configuration 1 of GDP in monomer *A* of structure DP (faded colors) is overlapped with the guanine base of GDP in monomer *B*, which adopts configuration 2. The active-site residues of monomer *B* and the nucleotide (bold colors) are shown. Note the displacement of the α-phosphate and the ribose ring between the two structures.

3.2. Nucleotide-binding configurations differ in both conformation and occupancy

In monomer *A* of structure DP, two conformations of the GDP (Fig. 1*a*) are each modeled at half occupancy. One, with the phosphate chain extended under the motif I P-loop ('conformation 1'), is similar to that seen in the structures of other GDP-bound GTPases (Tong *et al.*, 1991), generally in the presence of Mg^{2+} bound at the active site. The extended conformation 1 is reminiscent of that seen in the magnesium-free GDP complex of the SRP GTPase FtsY (Gawronski-Salerno *et al.*, 2007). The other conformation ('conformation 2') was observed in an earlier Mg^{2+}-free GDP-bound structure of the Ffh NG domain (PDB code 2ng1; Freymann *et al.*, 1999). The difference between the two lies in the relative orientations of the β-phosphate group, which in 2ng1 'flips out' from the P-loop and is directed towards the IBD and solvent (Freymann *et al.*, 1999). The two different conformations of GDP in monomer *A* have not previously been observed in the same crystal (Freymann *et al.*, 1999). Here, both configurations are well resolved (Fig. 1). However, there is no evidence for partial occupancy of the Mg^{2+} site (no magnesium was included in the crystallization conditions) and other than local shifts as discussed below there is little indication that the overall protein structures of the two GDP-binding states are globally different.

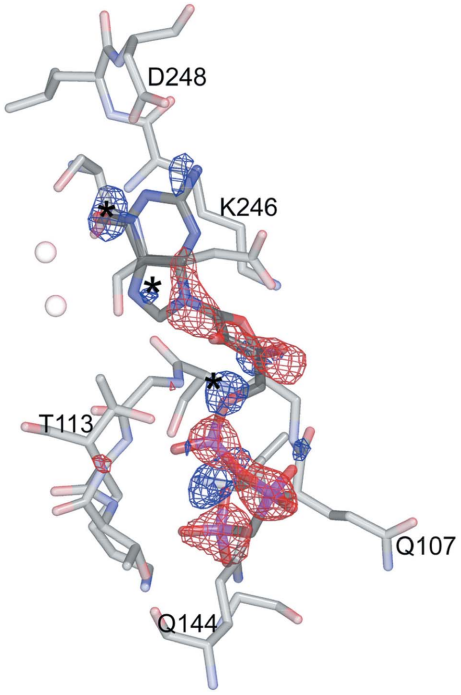

Figure 3
Water and nucleotide sites overlap. Difference maps calculated with bound nucleotide modeled at full and partial occupancy are shown. The GMPPCP of monomer *B* in structure PCP is partially occupied (~60%) and positive residual difference density peaks identify static water positions (*) identified previously in the structure of apo Ffh at 1.1 Å resolution (Ramirez & Freymann, 2006). When modeled at full occupancy, the nucleotide is traced by negative difference density (red, at -3σ).

The GDP is located in a pocket between Lys246 of motif IV, the closing loop (see below) and the buried invariant Lys117 which follows the P-loop on helix α1. Accompanying the rotation of the GDP β-phosphate in monomer *A*, the base is displaced by ~0.56 Å (Fig. 2*a*), with the ribose moving to accommodate the relative displacement between the guanine and phosphate groups of the bound nucleotide. These shifts are clearly supported by residual difference density when a single conformation is modeled; however, they are not fully resolved. The sliding of functional groups in the site, which is also evident in structure PCP, suggests that the two binding modes are not discrete. That is, the two modeled configurations convoluted with anisotropic temperature factors are likely to represent an envelope of the binding distribution within the site.

In contrast, in the *B* monomer of structure DP only one well defined conformation of GDP is observed, which corresponds to the 'flipped-out' conformation 2 observed in monomer *A* (Fig. 1*c*). Superimposition of the guanine base in monomer *B* with the extended GDP conformation of monomer *A* reveals shifts in the ribose group and α-phosphate (Fig. 2*c*) similar to those between the two conformations observed in monomer *A*, consistent with these shifts being intrinsic to accommodation of the positions of the phosphate chain in the two different binding states. The asymmetry in binding modes between monomers *A* and *B* is likely to arise from differences in the crystal-packing environment of the two monomers in the asymmetric unit (see below) and is echoed in structure PCP.

In both monomers of the GMPPCP complex structure, the nucleotide adopts the noncanonical conformation described previously in the structures of the GMPPNP-bound Ffh (PDB codes 1jpn and 1jpj; Padmanabhan & Freymann, 2001). This conformation is unique to SRP GTPases in that the β-phosphate rotates away from the P-loop (as observed in configuration 2 of the GDP-bound structure) and the γ-phosphate is turned back towards the P-loop (Padmanabhan & Freymann, 2001). In monomer *A* of structure PCP, similar to monomer *A* of structure DP, the nucleotide occupies at least two distinct positions. These are modeled as two configurations, each at 40% occupancy, such that the estimated occupancy of the site is 80% based on the flatness of residual difference maps. Again, however, these two positions are likely to represent an envelope of available binding configurations. The magnitudes of the shifts relative to the protein active-site frame are similar to those in monomer *A* of structure DP (Figs. 2*a* and 2*b*).

As in structure DP, there is only one binding configuration in monomer *B* of structure PCP, but in this case the GMPPCP is at only 60% occupancy (Figs. 1*d* and 3). Positive residual difference peaks of 4.2σ at the O6 of the guanine ring and 4.6σ between the O2C and O1A atoms and peaks between 3σ and 4σ near the N2 and N7 of the guanine base and C5* of the ribose in monomer *B* (Fig. 3) locate three water molecules identified in a structure of apo Ffh NG determined previously in the same crystal form (PDB code 2j45; Ramirez & Freymann, 2006). These waters were modeled at 40% occupancy and refine to temperature factors similar to those of the

nucleotide ligand. The resulting difference maps showed no significant residual peaks. At the protein structural level the overlap between the apo and GMPPCP-bound conformation is complete (the r.m.s.d. over 294 C^{α} atoms is 0.55 Å) and therefore the structure was also modeled as two chains: one GMPPCP-bound (60% occupancy) and one apo (40% occupancy).

3.3. Three flexible elements of the nucleotide-binding site

There are three regions of the GTPase active site that exhibit conformational variability directly associated with the observed variation in nucleotide-binding mode: these occur at the motif I P-loop, the closing loop and the buried Lys117 side chain (Fig. 4). The constriction between the bottom and top of the glycine-rich P-loop is found to be variable in the absence of bound ligand (Gariani *et al.*, 2005; Padmanabhan & Freymann, 2001). Superimposition of monomers *A* and *B* of structures DP or PCP on the P-loop (16 C^{α} atoms, residues 101–116) yields r.m.s.d.s of 0.18 and 0.29 Å, respectively, with the largest shifts in both comparisons (to 0.64 Å) occurring at Gln107, the residue at the 'top' of the P-loop 'jaws' (Padmanabhan & Freymann, 2001). In GDP conformation 1, the phosphate groups are closely packed between the main-chain atoms of these residues (a β-phosphate O atom rests 2.6 Å from Gly108 N) and relatively small differences in separation between monomers in the asymmetric unit are likely to impact on the adoption of one or the other phosphate configurations. Indeed, it was previously shown that the NG structure itself limits opening of the P-loop 'jaws' so that the GTP analog cannot adopt the canonical GTP-binding configuration (Focia, Shepotinovskaya *et al.*, 2004; Padmanabhan & Freymann, 2001), as also observed here in structure PCP.

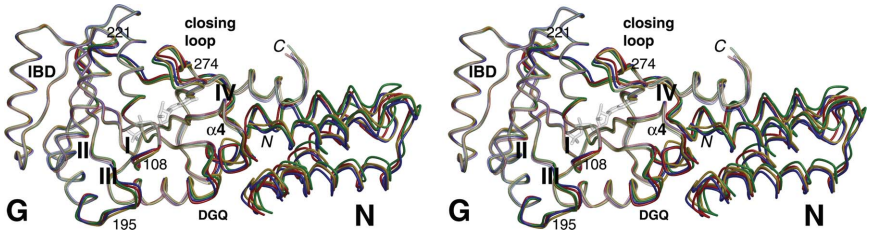

Figure 4
Conformational differences between the proteins are limited. Stereo diagrams of both monomers of structures DP and PCP superimposed on the C^{α} atoms of the G domains. The location of the binding site is indicated with a model of one conformation of the GDP in monomer *A* of structure DP. Monomer *A* of structure DP is shown in red and monomer *B* in blue; monomer *A* of structure PCP is shown in green and monomer *B* is shown in gold. Main-chain conformational differences among monomers of new structures occur at the NG-domain interface and five discrete regions in the G domain.

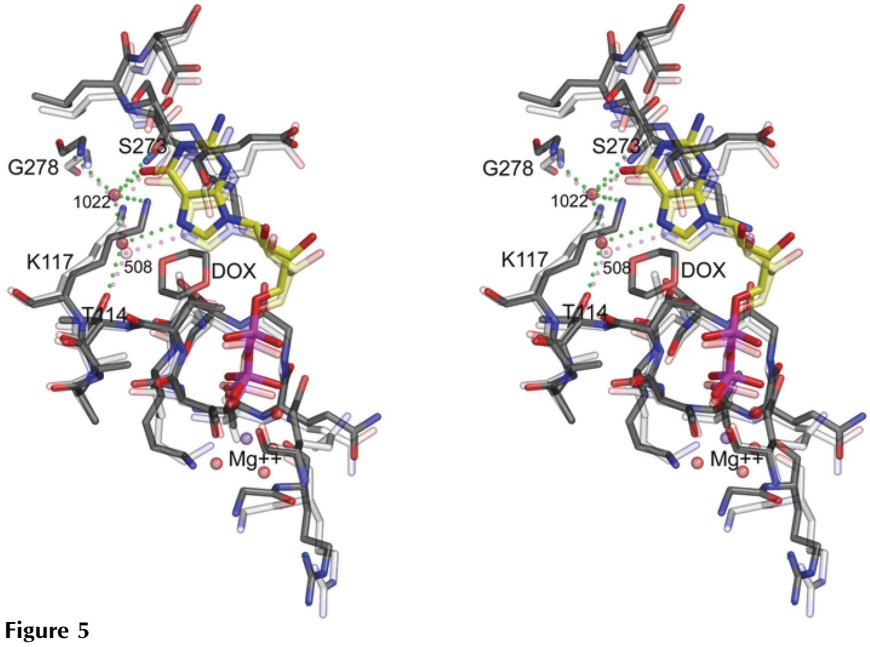

Figure 5
The buried Lys117 contributes to nucleotide accommodation. A stereo diagram of the active site of monomer *A* of structure DP (bold colors) superimposed on the active site of structure 1ng1 (Mg^{2+}-GDP Ffh NG; faded colors). Nucleotides and surrounding residues are shown with hydrogen-bonding interactions between two waters and Lys117 of monomer *A* of structure DP drawn as green dotted lines and those between one water and Lys117 of 1ng1 shown in faded magenta. A dioxane molecule (labeled 'DOX') in the active site of structure DP may stabilize Lys117 in a single conformation.

The second element is the closing loop, a dynamic structure that is unique to the SRP GTPases (Freymann *et al.*, 1999) and packs against the guanine base, apparently serving to facilitate nucleotide exchange (Freymann *et al.*, 1999) and, here, shifts in position of the bound nucleotide. Thus, the rearrangements of the guanine base, ribose and phosphates that occur between the two conformations of GDP and GMPPCP in monomer *A* of structures DP and PCP, respectively, are accompanied by shifts in the closing loop. These are modeled by disorder and the adoption of at least two conformations by residues in the loop. In contrast, in monomer *B* of structure DP only one conformation is observed. (The conformation may also be stabilized by a bound dioxane molecule; see below.) In the structure PCP, which represents the superposition of two binding states, again at least two conformations of the closing loop are observed.

The third element is the buried Lys117 side chain that exhibits distinct corresponding conformational states, adopting a different position in monomer *A* of structure DP from that observed in previous structures of the MgGDP complex. This also impacts the water structure in the active site. In monomer *A* of structure DP, two water molecules bridge the side chain of Thr114 with Lys117, rather than one as observed in the previous structure 1ng1 (Freymann *et al.*, 1999). In monomer *B* Lys117 adopts two alternate conformations, one similar to the

Table 2
R.m.s.d. values and displacements (Å) for regions of the G domains.

Region (residues)	GDP *A*/*B* monomers	GMPPCP *A*/*B* monomers	GDP *A* on GMPPCP *A*	GDP *B* on GMPPCP *B*
P-loop (105–117) r.m.s.d.	0.175	0.290	0.282	0.392
Displacement				
Motif I Gln107	0.30	0.64	0.63	0.88
G domain (99–271) r.m.s.d.	0.326	0.499	0.449	0.586
Displacements				
IBD loop 149–151	0.48	1.10	0.34	1.46
Motif III 190–199	0.39	0.99	0.55	0.89
DGQ motif 222–226	0.45	0.59	0.95	0.82
DARGG loop (250–262)	0.53	1.05	0.88	0.86

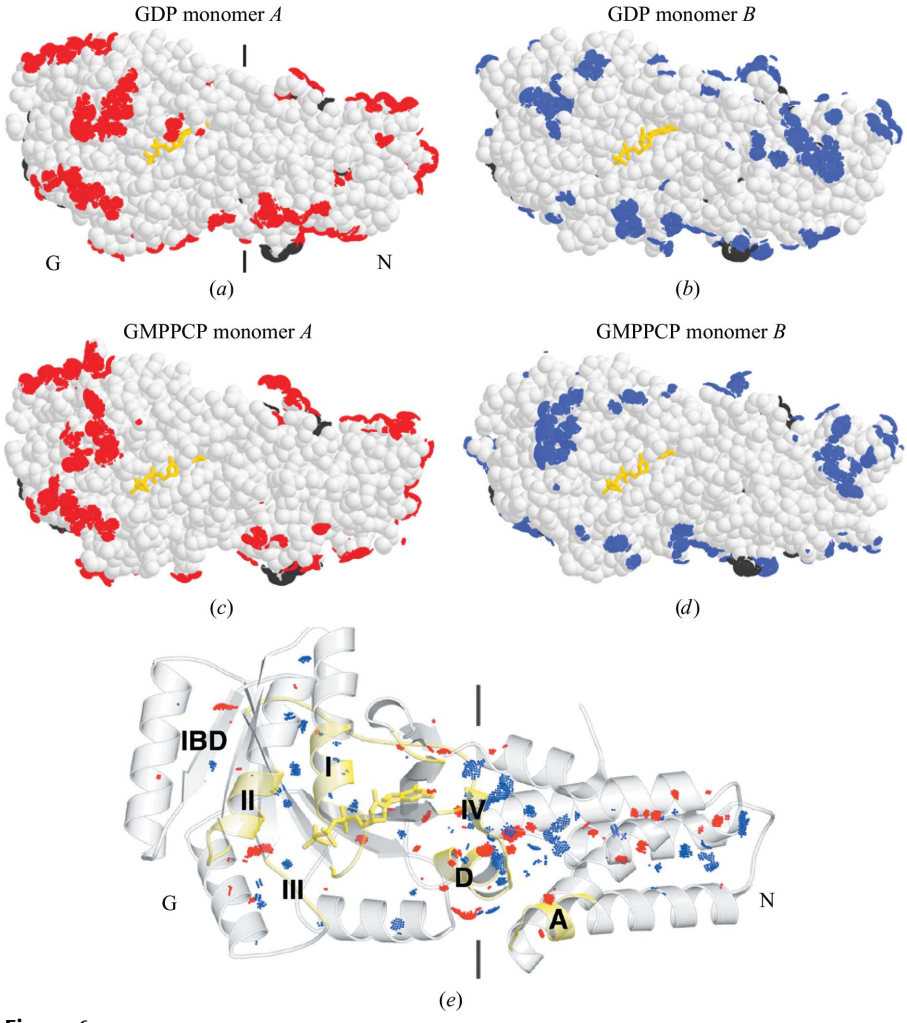

Figure 6
Shared and unique packing interfaces for the two monomers in the asymmetric unit. The locations of the N and G domains are indicated and a vertical black line indicates the approximate location of the NG interface. The position of the nucleotide is indicated in yellow. (*a*) Crystal-packing interactions unique to monomer *A* of structure DP are shown in red along the surface of the molecule. (*b*) Crystal-packing interactions unique to monomer *B* of structure DP are shown in blue. (*c*) Crystal-packing interactions unique to monomer *A* of structure PCP are shown in red. (*d*) Crystal-packing interactions unique to monomer *B* of structure PCP are shown in blue. Crystal packing was evaluated using *PROBE* (Word, 2000). A 180° rotation around a horizontal axis yields a common packing interface that is shared by all monomers in these crystal forms (not shown; Ramirez & Freymann, 2006). (*e*) Differences in intramolecular protein–protein packing interactions between the two monomers of structure DP and structure PCP. The orientation of the ribbon diagram is the same as for the surface diagrams above. GTPase conserved motifs are indicated with roman numerals I–IV; SRP GTPase conserved motifs ALLEADV and DARGG that span the N/G interface are indicated by the letters A and D, respectively.

conformation in monomer *A* and the other as observed in 1ng1, with corresponding changes in the occupancy of the bridging second water molecule (Wat1022; Figs. 2*b* and 5). Thus, the packing of the closing loop yields an open configuration at the base of the binding site such that there is sufficient volume to accommodate distinct lysine and water positions.

A well ordered dioxane molecule is packed between Pro276 of the closing loop and Leu148 in monomer *A*, but is not present in monomer *B* of structure DP. The asymmetry is significant because eight other dioxane molecules not located at crystal contacts occupy four equivalent positions in the *A* and *B* monomers. The dioxane molecule is in close proximity to the side chain of Lys117 of monomer *A*, perhaps stabilizing it in the observed conformation (Fig. 5).

3.4. A role for crystal packing

For each structure described here, the distinct binding configurations observed in the two monomers of each asymmetric unit may ultimately arise from differences in packing environment. Importantly, the structural elements discussed in the previous section are not directly involved in packing interactions and therefore it becomes of interest to try to dissect how different crystal-packing interactions act allosterically to impact on nucleotide-binding configuration. The packing environments were evaluated using *PROBE* (Word, Lovell, LaBean *et al.*, 1999; Word, Lovell, Richardson *et al.*, 1999), identifying ∼36% of residues in each monomer of structure DP and ∼30% of residues of each monomer in structure PCP as involved in protein–protein or protein–nucleotide crystal contacts (Fig. 6). Of these, however, only two-thirds (representing ∼20% of all residues) are unique to each monomer because a twofold symmetric crystallographic head-to-tail crystal-packing interface is common to each monomer (Ramirez & Freymann, 2006). These unique interactions, comprising some 60–70 residues in each case, must affect the differences in nucleotide binding

that are observed. Differences between the protein structures that can be directly related to differences in crystal-packing interactions are localized primarily to the N domains, which are displaced differently relative to the positions of the G domains in each monomer of the asymmetric unit, and to five regions of the G domain (Figs. 4 and 6, and Table 2). Of these, the DGQ loop between β4 and α3, the DARGG motif and helix α4 and the C-terminal residues are near the N/G-domain interface. The two others are distal to the nucleotide-binding pocket, the first in the loop between helix α1a and strand β2b of the IBD and the second in the conserved GTPase motif III. The conformations of these regions are more similar between the *A* monomers of both structures DP and PCP and differ between the *A* and *B* monomers in each crystal. A final region is the closing loop, as discussed above.

Maps of intramolecular packing interactions excluding surface residues were generated for each molecule in the asymmetric unit (Word, Lovell, LaBean *et al.*, 1999; Word, Lovell, Richardson *et al.*, 1999) and the differences in packing density are illustrated in Fig. 6(*e*). The greatest density of differences in packing are located at the N/G interface, reflecting differences in the relative orientations of the two domains within the inter-domain interface, which was previously shown to be flexible (Ramirez *et al.*, 2002). A tightening of the packing relationship between the IBD and the motif I/helix α1 region in the *B* monomers (highlighted in blue in Fig. 6*e*) may be related to the restriction in configuration and occupancy of the nucleotide bound in *B* monomers relative to those observed in the *A* monomers of each crystal. The greatest density of intramolecular packing differences between the monomers of structures DP and PCP is located at the N/G-domain interface, supporting the notion that the N domain can function as either a sensor or regulator of nucleotide occupancy as well as binding configuration (Freymann *et al.*, 1997; Montoya *et al.*, 1997).

3.5. Crystallographic observation of dynamic binding configurations

Simultaneous observation of shifts in nucleotide-binding configuration and position relative to the protein observed in the high-resolution structures DP and PCP demonstrate directly that nucleotide binding to the SRP GTPase Ffh is not static but is rather dynamic. At lower resolution, similar shifts in binding mode have been inferred from comparison of different structures of the related GTPase FtsY (Gawronski-Salerno *et al.*, 2007). In the *B* monomers of structures DP and PCP the nucleotides occur in only one configuration, an effect that is likely to arise owing to a particular crystal-packing environment. The shifts of the nucleotide that are observed within monomer *A* and between monomers *A* and *B* can be inferred to be coordinated to subtle protein 'breathing' motions, which have been shown in other systems to redistribute on binding ligand (Lewis *et al.*, 1998; Reisdorph *et al.*, 2003). The differences in packing density at the N/G interface may also reflect such a redistribution, although the direct relationship with binding configuration is difficult to establish and would require additional structures in different space groups and packing environments.

Previously, a 2.0 Å resolution GDP-bound structure of Ffh (PDB code 2ng1) was determined from crystals grown under conditions similar to those for structure DP, but which exhibited a different crystal form with only one monomer in its asymmetric unit. However, the crystal packing is very similar to monomer *A* in structure DP, differing primarily only at the closing loop and motif IV (there being no 'monomer *B*') and also in regions of the N domain and N/G-domain interface. This structure was interpreted in terms of a single conformation for GDP (Freymann *et al.*, 1999) which is the same as configuration 2 observed at partial occupancy in monomer *A* and at full occupancy in monomer *B* of structure DP. The structure of the G domain in 2ng1 is equally comparable to either of the two monomers of structure DP (with r.m.s.d.s of 0.576 Å over 172 C^{α} atoms for 2ng1 monomer *A* and 0.577 Å for 2ng1 monomer *B*). In 2ng1, an ethylene glycol molecule from the cryoprotectant overlaps the position of dioxane in monomer *A* of structure DP. However, while there is no evidence in the lower resolution structure for alternate configurations of the bound nucleotide, there is evidence for disorder near the buried Lys117, which may indicate that Lys117 assumes the same second conformation in 2ng1 as in monomer *B* of structure DP.

A previously determined 1.9 Å resolution structure of Ffh NG with the nonhydrolysable GTP analog GMPPNP bound (PDB code 1jpn) also exhibited ambiguities in binding mode that were not fully interpretable at that resolution. The crystal was obtained under almost identical conditions and in the same crystal form as the crystals yielding structure PCP. In 1jpn the GMPPNP molecule is modeled at full occupancy in monomer *A* and although there was evidence for partial occupancy of the GMPPNP molecule in monomer *B*, no alternate nucleotide or protein conformations could be built. The protein structure is very similar to structure PCP, with an r.m.s.d. of 0.297 Å over 296 C^{α} atoms upon overlap of the *A* monomers and 0.312 Å upon overlap of the same region of the *B* monomers. Interestingly, the two configurations of GMPPCP resolved in monomer *A* of structure PCP bracket the single position of GMPPNP modeled in monomer *A* of the lower resolution structure 1jpn.

3.6. Implications for understanding the dynamic nucleotide binding of the SRP GTPase

The ultrahigh-resolution structures of the nucleotide complexes reported here demonstrate that binding configurations determined in lower resolution structures may obscure distinct positional and conformational differences and represent averages across space and occupancy. The simple interpretation of binding modes obtained from lower resolution structures must therefore be tempered and the observation of flexibility in the position and orientation of the bound nucleotide prompts a need for recognition that the 'GDP-bound' or 'GTP-bound' state of the SRP GTPase is necessarily heterogeneous. Such heterogeneity is not often reported in

structures of other GTPases, even those determined at ultra-high resolution (Ramirez, unpublished work). However, these observations may be relevant to the degeneracy in nucleotide-binding specificity demonstrated biochemically for *E. coli* FtsY (Shan & Walter, 2003) and to the structural degeneracy of the binding mode observed in the structure of a recently reported *E. coli* FtsY nucleotide complex (Reyes *et al.*, 2007). The binding mode for magnesium-free GDP (Freymann *et al.*, 1999) may be energetically favorable and functionally important for the SRP GTPases (Focia, Alam *et al.*, 2004; Padmanabhan & Freymann, 2001; Reyes *et al.*, 2007). Furthermore, the structural elements that accommodate distinct nucleotide-binding configurations may be important in maintaining the GTPase in an 'off' but primed state when GTP binds to the monomeric proteins (Padmanabhan & Freymann, 2001; Rapiejko & Gilmore, 1997; Song *et al.*, 2000). It remains to be determined how this behavior may facilitate the interaction (or reflect the structural requirements) of the two SRP GTPases during assembly of their heterodimeric complex, in which the two buried nucleotides are bound at full occupancy and in the canonical configuration (Egea *et al.*, 2004; Focia, Shepotinovskaya *et al.*, 2004; Shan *et al.*, 2007).

We acknowledge the contribution of Anita M. Preininger in the the early stages of the work and thank Yi Fan and Irina Shepotinovskaya for technical assistance, Robert Ramirez for advice with script programming and figures, and Erica McCabe for editorial assistance. This work was supported by grant GM058500 from the NIH. Use of the Advanced Photon Source was supported by the US Department of Energy, Basic Energy Sciences, Office of Science under Contract No. W-31-109-Eng-38. Use of the BioCARS Sector 14 was supported by the National Institutes of Health, National Center for Research Resources under grant No. RR07707. Portions of this work were performed at DuPont–Northwestern–Dow Collaborative Access Team (DND-CAT) Sector 5. DND-CAT is supported by E. I. DuPont de Nemours & Co., The Dow Chemical Company and the State of Illinois. Use of the APS was supported by the US Department of Energy, Office of Science, Office of Basic Energy Sciences under Contract No. DE-AC02-06CH11357. DMF and UDR measured the diffraction data, UDR carried out initial model building and refinement, developed the computational tools and wrote the manuscript, and DMF and PJF revised the manuscript.

References

Bourne, H. R., Sanders, D. A. & McCormick, F. (1991). *Nature (London)*, **349**, 117–127.

Burmeister, W. P. (2000). *Acta Cryst.* D**56**, 328–341.

Collaborative Computational Project, Number 4 (1994). *Acta Cryst.* D**50**, 760–763.

DePristo, M. A., de Bakker, P. I. & Blundell, T. L. (2004). *Structure*, **12**, 831–838.

Egea, P. F., Shan, S. O., Napetschnig, J., Savage, D. F., Walter, P. & Stroud, R. M. (2004). *Nature (London)*, **427**, 215–221.

Focia, P. J., Alam, H., Lu, T., Ramirez, U. D. & Freymann, D. M. (2004). *Proteins*, **54**, 222–230.

Focia, P. J., Shepotinovskaya, I. V., Seidler, J. A. & Freymann, D. M. (2004). *Science*, **303**, 373–377.

Freymann, D. M., Keenan, R. J., Stroud, R. M. & Walter, P. (1997). *Nature (London)*, **385**, 361–364.

Freymann, D. M., Keenan, R. J., Stroud, R. M. & Walter, P. (1999). *Nature Struct. Biol.* **6**, 793–801.

Gariani, T., Samuelsson, T. & Sauer-Eriksson, A. E. (2005). *J. Struct. Biol.* **153**, 85–96.

Gawronski-Salerno, J., Coon, V. J., Focia, P. J. & Freymann, D. M. (2007). *Proteins*, **66**, 984–995.

Jones, T. A., Zou, J.-Y., Cowan, S. W. & Kjeldgaard, M. (1991). *Acta Cryst.* A**47**, 110–119.

Keenan, R. J., Freymann, D. M., Stroud, R. M. & Walter, P. (2001). *Annu. Rev. Biochem.* **70**, 755–775.

Kleywegt, G. J. & Jones, T. A. (1997). *Methods Enzymol.* **277**, 525–545.

Kleywegt, G. J., Zou, J. Y., Kjeldgaard, M. & Jones, T. A. (2001). *International Tables for Crystallography*, Vol. F, edited by M. G. Rossmann & E. Arnold, pp. 353–356. Dordrecht: Kluwer Academic Publishers.

Kraulis, P. J. (1991). *J. Appl. Cryst.* **24**, 946–950.

Lamzin, V. S., Perrakis, A. & Wilson, K. S. (2001). *International Tables for Crystallography*, Vol. F, edited by M. G. Rossmann & E. Arnold, pp. 720–722. Dordrecht: Kluwer Academic Publishers.

Lewis, J. K., Bothner, B., Smith, T. J. & Siuzdak, G. (1998). *Proc. Natl Acad. Sci. USA*, **95**, 6774–6778.

Lovell, S. C., Davis, I. W., Arendall, W. B. III, de Bakker, P. I., Word, J. M., Prisant, M. G., Richardson, J. S. & Richardson, D. C. (2003). *Proteins*, **50**, 437–450.

Lovell, S. C., Word, J. M., Richardson, J. S. & Richardson, D. C. (1999). *Proc. Natl Acad. Sci. USA*, **96**, 400–405.

Luirink, J. & Dobberstein, B. (1994). *Mol. Microbiol.* **11**, 9–13.

Luirink, J. & Sinning, I. (2004). *Biochim. Biophys. Acta*, **1694**, 17–35.

Merritt, E. A. & Bacon, D. J. (1997). *Methods Enzymol.* **277**, 505–524.

Montoya, G., Svensson, C., Luirink, J. & Sinning, I. (1997). *Nature (London)*, **385**, 365–369.

Murshudov, G. N., Vagin, A. A. & Dodson, E. J. (1997). *Acta Cryst.* D**53**, 240–255.

Murshudov, G. N., Vagin, A. A., Lebedev, A., Wilson, K. S. & Dodson, E. J. (1999). *Acta Cryst.* D**55**, 247–255.

Otwinowski, Z. (1993). *Proceedings of the CCP4 Study Weekend. Data Collection and Processing*, edited by L. Sawyer, N. W. Isaacs & S. Bailey, pp. 55–62. Warrington: Daresbury Laboratory.

Padmanabhan, S. & Freymann, D. M. (2001). *Structure*, **9**, 859–867.

Perrakis, A., Morris, R. & Lamzin, V. S. (1999). *Nature Struct. Biol.* **6**, 458–463.

Pool, M. R. (2005). *Mol. Membr. Biol.* **22**, 3–15.

Ramirez, U. D. & Freymann, D. M. (2006). *Acta Cryst.* D**62**, 1520–1534.

Ramirez, U. D., Minasov, G., Focia, P. J., Stroud, R. M., Walter, P., Kuhn, P. & Freymann, D. M. (2002). *J. Mol. Biol.* **320**, 783–799.

Rapiejko, P. J. & Gilmore, R. (1997). *Cell*, **89**, 703–713.

Reisdorph, N., Thomas, J. J., Katpally, U., Chase, E., Harris, K., Siuzdak, G. & Smith, T. J. (2003). *Virology*, **314**, 34–44.

Reyes, C. L., Rutenber, E., Walter, P. & Stroud, R. M. (2007). *PLoS ONE*, **2**, e607.

Schneider, T. R. (1996). *Proceedings of the CCP4 Study Weekend. Macromolecular Refinement*, edited by E. Dodson, M. Moore, A. Ralph & S. Bailey, pp. 133–144. Warrington: Daresbury Laboratory.

Shan, S. O., Chandrasekar, S. & Walter, P. (2007). *J. Cell Biol.* **178**, 611–620.

Shan, S. O. & Walter, P. (2003). *Proc. Natl Acad. Sci. USA*, **100**, 4480–4485.

Shepotinovskaya, I. V., Focia, P. J. & Freymann, D. M. (2003). *Acta Cryst.* D**59**, 1834–1837.

Song, W., Raden, D., Mandon, E. C. & Gilmore, R. (2000). *Cell*, **100**, 333–343.
Stura, E. A. & Wilson, I. A. (1990). *Methods*, **1**, 38–49.
Stura, E. A. & Wilson, I. A. (1991). *J. Cryst. Growth*, **110**, 270–282.
Teng, T.-Y. (1990). *J. Appl. Cryst.* **23**, 387–391.
Teng, T.-Y. & Moffat, K. (2002). *J. Synchrotron Rad.* **9**, 198–201.
Tong, L. A., de Vos, A. M., Milburn, M. V. & Kim, S.-H. (1991). *J. Mol. Biol.* **217**, 503–516.
Walsh, M. A., Schneider, T. R., Sieker, L. C., Dauter, Z., Lamzin, V. S. & Wilson, K. S. (1998). *Acta Cryst.* D**54,** 522–546.
Weik, M., Ravelli, R. B., Kryger, G., McSweeney, S., Raves, M. L., Harel, M., Gros, P., Silman, I., Kroon, J. & Sussman, J. L. (2000). *Proc. Natl Acad. Sci. USA*, **97**, 623–628.
Wittinghofer, A. & Gierschik, P. (2000). *Biol. Chem.* **381**, 355.
Word, J. (2000). Thesis. Duke University.
Word, J. M., Lovell, S. C., LaBean, T. H., Taylor, H. C., Zalis, M. E., Presley, B. K., Richardson, J. S. & Richardson, D. C. (1999). *J. Mol. Biol.* **285**, 1711–1733.
Word, J. M., Lovell, S. C., Richardson, J. S. & Richardson, D. C. (1999). *J. Mol. Biol.* **285**, 1735–1747.